Wave-Induced Drift Force in the Marginal Ice Zone

DIANE MASSON

Institute of Ocean Sciences, Sidney, BC, Canada

(Manuscript received 30 October 1989, in final form 16 January 1990)

ABSTRACT

Wind waves are commonly ignored when modeling the ice motion in the marginal ice zone. In order to estimate the importance of the wave forcing, an expression for the second-order wave-induced drift force on a floe exposed to a full directional wave spectrum is obtained in terms of a quadratic transfer function. For a given floe shape, the transfer function generally augments with the incident wave frequency, with a sharp increase near the resonant frequency of the pitch motion. The short wave limit of this function is determined by the shape of the horizontal contour of the floe. The value corresponding to the truncated cylindrical floe used here is two-thirds of the value obtained by the two-dimensional approximation. The total drift force is computed for two situations: an off-ice wind over a large polynya, and an on-ice wind at the extreme ice edge. In the first case, the drift force induced by the short fetch waves represents a significant fraction of the direct wind forcing and may be partly responsible for the formation of ice edge bands. In the second case, the very large drift force on a floe exposed to the high frequency components of the open water spectrum rapidly decreases (in the first few hundred meters) as these short waves are efficiently attenuated by the ice. This rapid decrease of the force generates a large compressive stress that is important in compacting the ice at the extreme ice edge.

1. Introduction

The drift of a body floating freely on the ocean surface is generally governed by wind, current, and waves. Under the assumption that wind and current actions dominate, a wave–ice interaction term has been commonly omitted in modeling sea ice motion in the marginal ice zone (MIZ) (e.g., Bruno and Madsen 1989) or the trajectory of iceberg drift (e.g., Smith and Donaldson 1987). However, some successful attempts have been made in the past to include such a term in the sea ice momentum balance. Hsiung and Aboul-Azm (1982) significantly improved iceberg drift trajectory predictions by including a wave radiation pressure term in the equation of motion for the iceberg. Wadhams (1983) showed that, in the outer part of the MIZ, the short waves generated in polynyas opened by an off-ice wind could be partly responsible for the formation of ice edge bands.

A floating ice mass exposed to waves undergoes oscillatory motions and also experiences a net drift forced by two wave related phenomena: the Stokes drift, which is a consequence of the wave-induced water particle orbits not being closed, and the net drift force due to the hydrodynamic impact of the waves. It is the latter force that is the focus of this paper. This is not to imply that the Stokes drift is negligible. Jenkins (1987) has shown, for example, that the surface Stokes drift can be up to 1% of the wind speed, for a wind of 10 m s^{-1}.

The magnitude of the wave-induced drift force depends on the floe shape and on its horizontal dimension relative to the incident wavelength. It is also a function of the directional spectral density of the incident wave field. Using three-dimensional potential theory, an expression for the wave-induced drift force on a vertically axisymmetric floe is derived herein. The general theory is first described for a single incident plane wave and then extended to a full directional wave spectrum. Kobayashi and Frankenstein (1987) estimated the monochromatic force using a similar approach. The drift force due to a single wave component is recomputed here, with a more detailed analysis of the frequency dependence of the force, and some clarification on the short wave limit as there was some confusion in their work about the appropriateness of this limit. The total force due to a full directional spectrum is then evaluated in two situations frequently occurring in the MIZ: when the wind blows over a large polynya opened by an off-ice wind, and when an on-ice wind blows over the ice edge. Finally, an attempt is made to estimate the drift force and the associated compressive stress on the ice as the open-water waves penetrate in the partially ice-covered waters of the MIZ.

2. Theoretical formulation

The hydrodynamic force acting upon a rigid body floating in waves is composed of a first-order (in wave slope) periodic term linearly dependent on the wave

Corresponding author address: Dr. Diane Masson, Institute of Ocean Sciences, P.O. Box 6000, Sidney, B.C., Canada, V8L 4B2.

amplitude, and a second-order nonlinear term proportional to the square of the wave amplitude. This second-order term includes a component independent of time, the drift force, and a slowly varying force which occurs at the difference frequencies between the various wave components. The mean horizontal force for the two-dimensional (2D) case has been examined by Longuet-Higgins (1977). In this approximation, the two-dimensional incident wave is transmitted or reflected only in the plus or minus incident direction, respectively. He showed that the drift force on a two-dimensional obstacle in normally incident waves can be written in terms of the incident, reflected, and transmitted wave amplitudes, A, A', and B, respectively. In deep water, the force per unit width, F', is

$$F' = \rho g(A^2 + A'^2 - B^2)/4 \quad (1)$$

where ρ is the density of water and g the gravity. Wadhams (1983) used this 2D approximation to estimate the magnitude of the wave radiation pressure on the floes.

In general, a floating object both diffracts and scatters incoming wave energy in all directions. Formulas for the drift force on three-dimensional bodies were first derived by Maruo (1960) and extended by Newman (1967) to include the moment about the vertical axis. The derivation, based on momentum balance, is briefly described in the following text.

Assuming an ideal fluid and linearizing the motion, momentum relations are used to derive an expression for the drift force on a body with no forward velocity in terms of the far-field velocity potential. The fluid velocity vector, $\mathbf{u}$, can be written in terms of a velocity potential, Φ, with $\mathbf{u} = \nabla\Phi(x, y, z; t)$, where (x, y, z) are Cartesian coordinates with the z-axis positive upwards and $z = 0$ the plane of the undisturbed free surface, and the x-axis in the direction of the incident wave. The fluid motion is assumed harmonic in time, and to be the sum of the incident wave, ϕ_i, and a disturbance due to the presence of the body, ϕ_s:

$$\Phi = (\phi_i + \phi_s)e^{-i\omega t} \quad (2)$$

where ω is the angular frequency. The linearized incident potential for a plane wave of amplitude $H/2$ is

$$\phi_i = -\frac{igH}{2\omega}\frac{\cosh[k(z+h)]}{\cosh(kh)}e^{ikx} \quad (3)$$

where k is the wavenumber with $k = \omega^2/g\tanh(kh)$, and h is the water depth. The disturbance potential can be treated linearly as the sum of the contributions from the diffraction of the incident wave on a fixed body, and the scattering by a body forced to oscillate in still water. For a body that is symmetric about the z-axis, the scattered waves are generated by the surge (back and forth), the heave (up and down), and the pitch (rotation about the y-axis) motions only. At a large distance from the body, this potential takes the form

$$\phi_s = -\frac{igH}{2\omega}\frac{\cosh[k(z+h)]}{\cosh(kh)}D(f;\theta)r^{-1/2}e^{ikr} \quad (4)$$

where the wave frequency, $f = \omega/2\pi$, and (r, θ) are cylindrical coordinates with r measured radially from the z-axis and θ counterclockwise from the positive x-axis. The scattering coefficient, $D(f; \theta)$, gives the angular distribution of the sum of the diffracted and scattered waves. This coefficient is computed as in Masson and LeBlond (1989), following the method developed by Isaacson (1982) to calculate the response of an axisymmetric body. It should be noted that Kobayashi and Frankenstein (1987) estimated the scattering coefficient using a related approach in which, instead of solving for a source strength distribution function as in Isaacson (1982), the potential is directly obtained from the integral equation of the boundary condition at the submerged surface of the body.

The drift force on an arbitrary body can be expressed in terms of the far-field potential (4) by considering the rate of change of momentum within the fluid domain bounded by the body's wetted surface, the free surface, and a control surface at infinity. When the time averages are taken, and only the second-order terms are retained (see Newman 1967 for details), the magnitude of the wave-induced force in the direction of the incident wave takes the form

$$F = \frac{\rho g}{2}\left\{\frac{1}{2}\left[1 + \frac{2kh}{\sinh(2kh)}\right]\right\}\left(\frac{H}{2}\right)^2 \times \int_0^{2\pi} |D(f;\theta)|^2(1 - \cos\theta)d\theta. \quad (5)$$

Thus, the second-order drift force can be inferred from the first order or linearized far-field potential only.

In order to obtain the drift force on a floe under the action of a realistic sea state, the theory developed for a regular incident wave train must be extended to the case of an irregular sea. A complex wave field is assumed to be characterized by a sequence of regular wave trains distributed over frequency, f, and direction, θ. It is commonly represented in terms of its directional frequency spectrum, $E(f, \theta)$, giving the density of contributions to the total variance of the surface displacement, η, per unit area of the frequency direction space with

$$\overline{\eta^2} = \int_0^{2\pi}\int_0^{\infty} E(f, \theta)dfd\theta \quad (6)$$

where the overbar represents a time average. This directional spectral density is conveniently written in terms of a one-dimensional frequency spectrum, $E(f)$, and a directional spreading function, $G(f, \theta)$, symmetrical about a mean wave direction, θ_o,

$$E(f, \theta) = E(f)G(f, \theta - \theta_o). \quad (7)$$

Further assuming that each of the wave components imparts to the floe the same force which it would if it

was merely one regular wave, the total drift force corresponding to random unidirectional waves can be obtained by summing the contributions from all the components of the incident spectrum. Using (5) and (6), the magnitude of the total wave-induced drift force applied on a floe in the mean direction, $\theta_o = 0$, of an irregular sea, can be written as

$$F = \int_0^{2\pi} \int_0^{\infty} E(f, \theta)\, \mathrm{Tr}(f) df \cos\theta d\theta \qquad (8)$$

with the quadratic transfer function

$$\mathrm{Tr}(f) = \rho g \left\{ \frac{1}{2} \left[1 + \frac{2kh}{\sinh(2kh)} \right] \right\} \times \int_0^{2\pi} |D(f; \theta)|^2 (1 - \cos\theta) d\theta. \qquad (9)$$

For a given floe shape in deep water, the transfer function (9) is a function of frequency only, as the floe is assumed to be symmetric about the vertical axis. In the next section, the transfer function is computed for a series of frequencies and floe shapes, and then used to determine the total wave-induced drift force on a floe, given a specified sea state.

3. Results and discussion

The floes are represented here as truncated cylinders of radius $a = 10$ m, and draft $d = 0.3$, 2.0, and 3.0 m, in a water depth $h = 100$ m. For a given radius to draft ratio, the scattering coefficient in (9), and thus the transfer function itself, is a function of the horizontal dimension of the floe relative to the incident wavelength, $\lambda = 2\pi/k$, only. The nondimensionalized transfer function, $\mathrm{Tr}' = \mathrm{Tr}/\rho g a$, for these three floes is presented in Fig. 1 as a function of the nondimensional wavenumber ka. When waves are long relative to the floe dimension (small ka), the incident waves are barely affected by the presence of the floe, resulting in small transfer function magnitudes. As ka increases, the diffracted wave and the waves generated by the wave-induced motions of the floe slowly develop. Consequently, the scattering amplitude and the ability of the waves to push the floe gradually augment. At a certain value of ka, the transfer function rapidly increases to approach its short-wave asymptotic value of 1.33, which will be discussed later. Associated with this sudden change in the value of the transfer function, two secondary peaks are present for the two thicker floes. These peaks are caused by a resonance of the response in the heave and pitch motion of the floe, respectively. The ka value at which the transfer function increases significantly varies with the floe shape, decreasing as the draft increases.

The sharp transition from low to high values of the transfer function appears not to be linked to a sudden increase in the amplitude of the diffracted and three forced waves, but rather to the occurrence of the res-

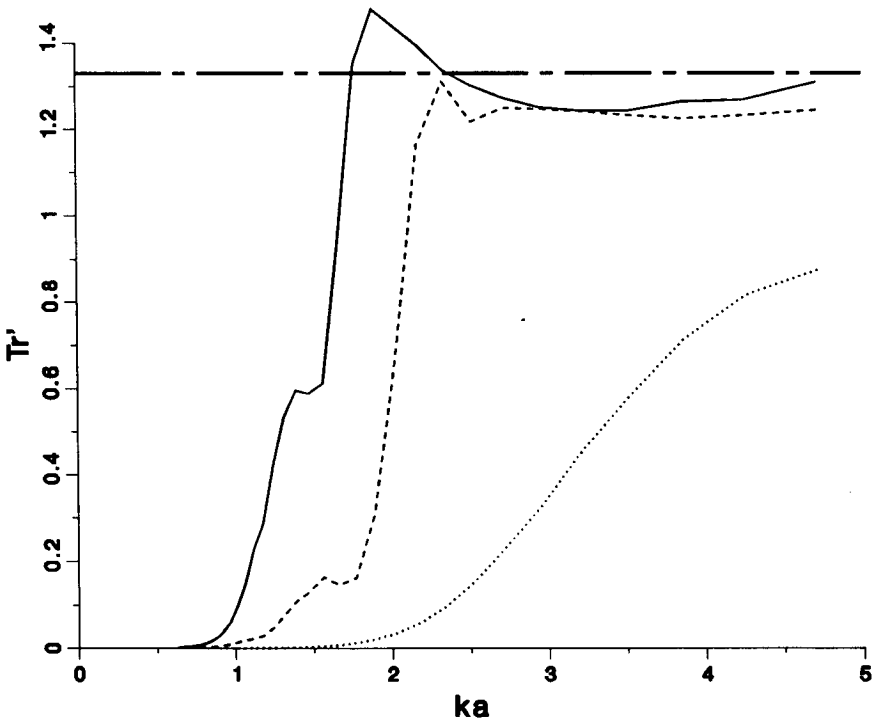

FIG. 1. Nondimensional transfer function, Tr', for floes of 10 m diameter and draft of 3 m (full line), 2 m (dashed line), and 0.3 m (dotted line) as a function of nondimensional wavenumber ka. The chain-dashed line indicates the short-wave limit value.

onant peak in the pitch motion. To illustrate this result, changes in the different components of the scattering coefficient of the backscattered wave, $D(f;\theta=\pi)$, are presented in Fig. 2 for the case $d = 3.0$ m. The magnitude (Fig. 2a) and the phase (Fig. 2b) of the four components are given for $ka = 1.0$–2.5. Although, for $1.0 \geqslant ka \geqslant 1.5$, the magnitude of the different components are relatively large, the total scattering coefficient remains small. For a value of ka just over 1.5, a 180° shift in the phase of the surge component, which is known to be linked to the appearance of the pitch resonant peak, allows the different components to interact in a more constructive way resulting in a large increase of the magnitude of the total scattering coefficient.

This result appears to be in agreement with the laboratory measurements of Harms (1987). In his experiment, the drift rate of 2D ice floe models in regular waves was measured at different wave periods, $T = 1/f$. A fundamentally different drift behavior was evident on either side of the pitch resonant peak period, delimiting a long-wave and short-wave drift regime. Given a constant wave height to wavelength ratio, the measured slope of the drift rate versus wave period curve was larger in the short-wave region than in the long-wave region. This experimental result is consistent with the sharp increase of the transfer function associated with the resonant peak of the pitch motion described above.

At large values of ka, the three forced waves are of small amplitude due to the vanishing wave-induced motions of the floe. The scattering coefficient is then dominated by the diffracted component. At the limit $ka \gg 1$, the diffracted wave separates into two parts: the reflected wave, and the shadow-forming wave which interferes with the incident wave to cancel the wave intensity behind the floe. The latter component does not contribute to the transfer function (9) as it travels along the positive x-axis ($\theta = 0$). The magnitude of the short-wave transfer function is therefore determined by the nature of the reflected wave. The short-wave limit of the wave-induced force on a three-dimensional body has been examined by Maruo (1960). He derived the limiting form of the drift force which can be written in terms of the nondimensional transfer function as

$$\mathrm{Tr}'_{\max} = \frac{1}{a}\int_{-a}^{+a} \sin^2\Theta dy, \quad \text{for} \quad ka \gg 1 \qquad (10)$$

where Θ is the angle that the tangent to the surface of the body makes with the direction of the incident wave, here the x-axis. According to (10), the limit value for the transfer function depends on the shape of the horizontal contour of the floe and its orientation relative to the heading angle of the incident wave. For a square floe, $\mathrm{Tr}'_{\max}$ takes the value of 2.0 and 1.0 when its forward face is perpendicular or at 45° with the incident wave direction, respectively. For the cylindrical floe used in this study, the nondimensional transfer function has short wave limit of 1.33 as shown in Fig. 1. Also, in this figure, the lower transfer function values of the thin floe, $d = 0.3$ m, demonstrate the effect of the limited draft that does not allow complete reflection of waves for which the momentum is distributed over a depth (of about half the wavelength, in deep water) exceeding the draft.

The two-dimensional approximation, in which all the reflected wave is assumed to travel backwards ($\theta = \pi$), is equivalent to the square floe, 0° heading angle case. In modeling the region of the MIZ near the ice edge, where the floes are of various shape and orientation, the 2D approximation undoubtedly leads to an overestimation of the wave-induced drift force. The value of 1.33 used here is more likely to represent a typical value of the transfer function. Kobayashi and Frankenstein (1987) obtained the same value for the drift force in very short waves by extrapolation of their numerical results, but without clearly demonstrating its validity.

So far, the drift force on a floe under the action of a monochromatic wave has been examined. The force due to a complete directional wave spectrum is now estimated using (8) and the previously computed values of the transfer function. Masson and LeBlond (1989) demonstrated that, in the MIZ, a wind blowing over areas covered by dispersed ice floes results in short and nearly isotropic wind waves. In this case, the wave-induced drift force, as given by (8), remains small because the wave energy is distributed almost equally over all directions. Thus, waves examined here are either short waves generated in polynyas inside the ice cover itself or open-water waves of various wavelengths incident on the ice edge and propagating into the ice cover. In the first situation, the development of the wave field is limited by the short fetch and may be specified in terms of the commonly used JONSWAP frequency spectrum Hasselman et al., 1973;

$$E(f) = \frac{\alpha g^2}{(2\pi)^4 f^5}\exp\left[-\frac{5}{4}\left(\frac{f}{f_0}\right)^{-4}\right] \times \gamma^{\exp[-(f-f_0)^2/(2\sigma^2 f_0^2)]} \qquad (11)$$

where

$$\sigma = \begin{cases} 0.07, & \text{for} \quad f \leqslant f_0 \\ 0.09, & \text{otherwise} \end{cases}$$

f_0 is the frequency at the maximum of the spectrum and is related to the fetch, X (m), and wind speed U (m s^{-1}), by $(Uf_0/g) = 3.5(gX/U^2)^{-0.33}$, α is the fetch dependent parameter equivalent to the Phillips' constant, $\alpha = 0.076(gX/U^2)^{-0.22}$, and finally $\gamma = 3.3$ is the peak enhancement factor. The spreading function in (7) is of the form $G(f,\theta) = I(s)\cos^{2s}(\theta/2)$, with $I(s)$ the normalization factor to ensure that $\int_0^{2\pi} G(f,\theta) \times d\theta = 1$, and s the spread parameter as given by Has-

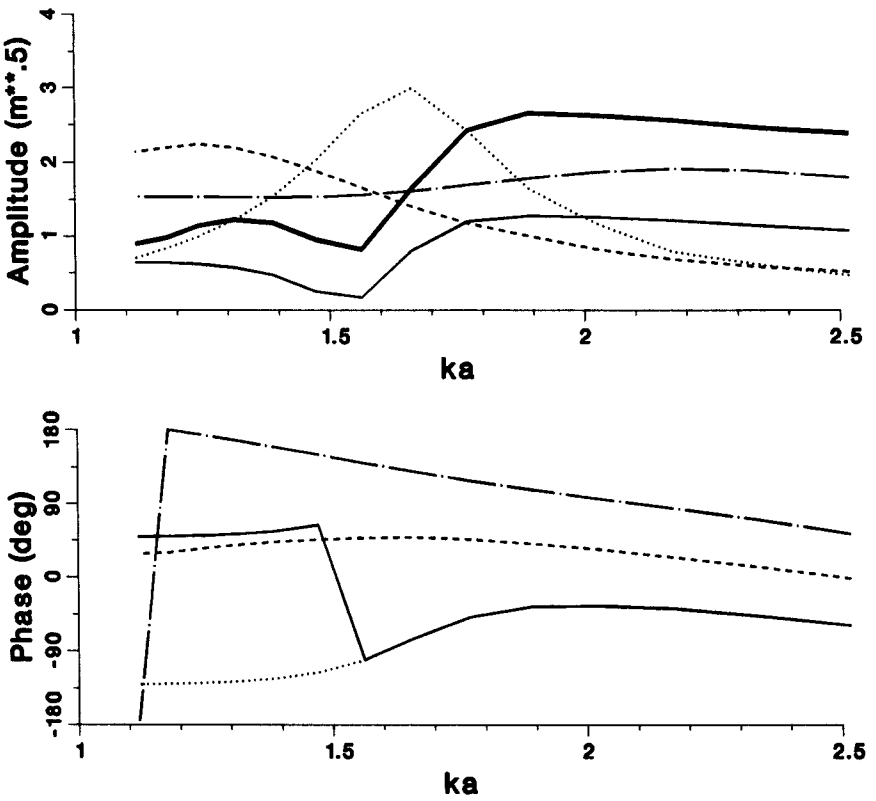

FIG. 2. Amplitude (a) and phase (b) of the component of the scattering coefficient at $\theta = \pi$ due to surge (full line), heave (dashed line), pitch (dotted line), and diffraction (chain-dotted line) versus nondimensional wavenumber ka. In (a) the thick full line gives the amplitude of the total scattering coefficient.

selmann et al. (1980): $s = 6.97(f/f_0)^{4.06}$ for $f < f_0$, and $s = 9.77(f/f_o)^{\nu}$ for $f \geqslant f_o$, with $\nu = [-2.33 - 1.45(U/c_o - 1.17)]$ and c_o is the phase velocity of the wave at the peak. This directional distribution reflects the known spectral broadening with increasing frequency, and with increasing U/c_o, above the peak frequency. The U/c_o dependence, commonly omitted, is retained here because of its large effect on the directional spread of the very "young" sea analyzed below.

Because of the short fetch (downwind extent) associated with open water leads inside the MIZ, the sea state is composed of very short period waves. Although the amplitude of these short waves is small, being limited by breaking, the asssociated high transfer function value results in a wave-induced drift force of magnitude comparable to the wind drag given by

$$F_a = \rho_a C_a A U^2 \qquad (12)$$

where ρ_a is the air density, C_a the air draft coefficient, and $A = \pi a^2$ the surface area of the floe. For typical values of $\rho_a = 1.2$ kg m^{-3} and $C_a = 3.0 \times 10^{-3}$, a wind speed $U = 10$ m s^{-1} generates on a 10 m diameter and 2 m draft floe a wind forcing $F_a = 113$ N. The same wind blowing over a polynya of 500 m fetch generates a wave field with $f_o = 0.95$ Hz. The drift force on the floe located at the downwind end of the lead is, according to (8), 62 N. The magnitude of the force is reduced here to 52% of the equivalent force obtained using the 2D approximation, mainly because of the transfer function being two-thirds of its equivalent 2D value, and to a lesser extent because of the multidirectionality of the waves given by the spreading function, $G(f, \theta)$. Thus, as suggested by Wadhams (1983), the wave-induced contribution, although smaller than the one that he estimated using the 2D approximation, appears to be a nonnegligible component of the ice momentum balance and could be partly responsible for the formation of ice edge bands.

When waves generated in the open water adjacent to the ice cover are impinging on the ice edge, an ice floe, located at the edge, is exposed to a wide range of wave frequencies. Assuming infinite fetch, the incident wave spectrum is now determined by the wind speed, U, and the duration, t, for which the wind has been blowing (time-limited situation). In Fig. 3, the spectral density and the corresponding wave-induced force contributions over frequency are given for a wind $U = 10$ m s^{-1}, a floe of draft $d = 2.0$ m, and a series of duration t from 1.7 to 20 hours. The wave spectrum is again given by (11) in which the fetch dependence

is now replaced by a time dependence for the peak frequency, $(Uf_o/g) = 16.8(gt/U)^{-3/7}$, and the Phillips-like constant, $\alpha = 0.203(gt/U)^{-2/7}$. At full development ($t \approx 20$ h), the wave spectrum takes the form of a Pierson–Moskowitch spectrum which is similar to (11) but without the effect of the peak enhancement factor ($\gamma = 1$).

Initially, the young sea state is composed of short waves which contribute to the drift force following the quadratic dependence of the force on the wave amplitude (times t_1, t_2 of Fig. 3). As the wave develops, the increasing spectral energy shifts to lower frequencies, and the spectral peak enters the small transfer function region (time t_3). The main contribution to the drift force now comes from frequencies larger than the peak frequency. At full development (time t_4), most of the energy of the spectrum is contained in a region where the transfer function is small. The total force is reduced, and is now entirely due to the high frequency tail of the wave spectrum. Also, comparing the different drift force contribution curves of Fig. 3, the effect of the frequency dependence of the spreading function on the drift force is evident. In the high-frequency spectral region, the same energy level at a given frequency results in a smaller drift force contribution for the "older" sea state, for which the spectral component has a larger directional spread (larger s value) being further away from the peak.

In the previous situation, the wave-induced drift force reaches a maximum value of about 7.0×10^3 N at a duration $t \approx 6$ h and then decreases to a value of 4.1×10^3 N for the fully developed sea. The same general development scheme would prevail for a different flow or a different wind speed. For example, a wind $U = 20$ m s^{-1} would generate a maximum force of 1.1×10^4 N after four hours, with a force at full wave development of 2.0×10^3 N. The total drift force for the fully developed sea is smaller for the stronger wind. In fact, the drift force at full development increases with wind speed because of the higher spectral energy content up to a point where the higher energy level can no longer compensate for the decreasing transfer function value. As a result of these two opposing effects, the wave-induced drift force at full development takes a maximum value of about 4.3×10^3 N for a wind speed $U \approx 9$ m s^{-1}. Such a wind generates, according to (12), a drag force on the floe of 92 N. This force is easily dwarfed by the wave-induced drift force at the extreme ice edge where the floes are directly exposed to the open water waves.

The waves, as they enter the ice cover, are significantly modified by the floes. Their energy follows an exponential decay, with an attenuation coefficient generally increasing with frequency, but with a slight decrease or "roll-over" at the highest frequencies. There is also evidence of a directional broadening of the spectrum as the waves penetrate the ice cover with the low-frequency broadening more slowly than the high-frequency components (Wadhams et al. 1986). In Table 1, typical values of the decay coefficient are given which have been estimated from data collected during the MIZEX-84 experiment and presented by Wadhams et

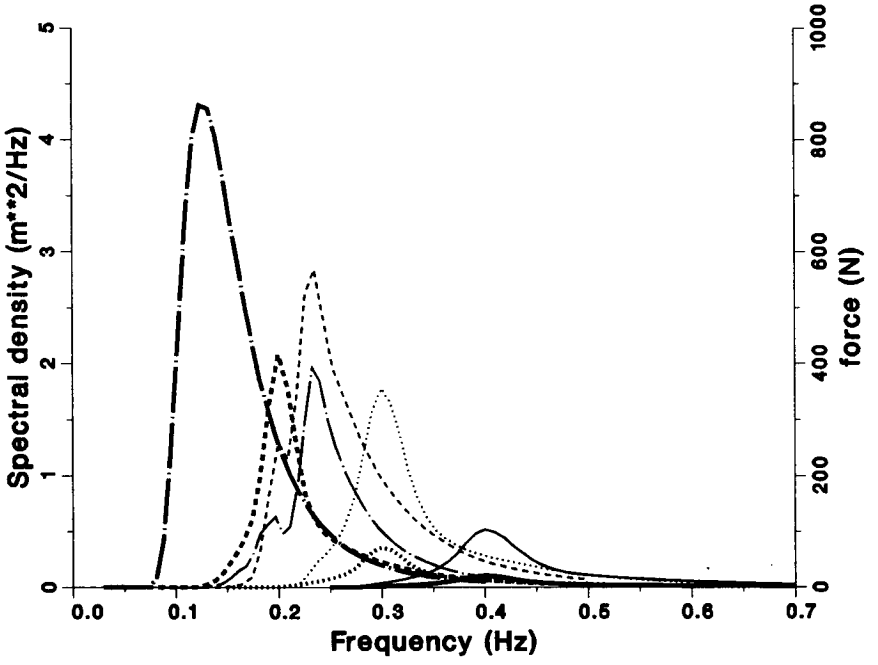

FIG. 3. Spectral density (thick lines) and wave-induced drift force (thin lines) when a wind $U = 10$ m s^{-1} has been blowing for $t_1 = 1.7$ h (full lines), $t_2 = 3.2$ h (dotted lines), $t_3 = 8.4$ h (dashed lines), and $t_4 = 20$ h (chain-dotted lines). The drift force is computed for a floe of 10 m diameter and 2 m draft.

TABLE 1. Attenuation coefficient, β, for a series of wave frequencies (estimated from Wadhams et al. 1986, Fig. 7).

Frequency (Hz)	β (10^{-4} m^{-1})
0.1	0.43
0.15	2.9
0.2	14.0
0.25	28.0
0.3	36.0
0.35	35.0
0.4	37.0
0.45	29.0
0.5	28.0

al. (1986) (their Fig. 7). As the open-water waves enter the ice cover, the high-frequency energy, which is responsible for most of the wave-induced drift force, rapidly decays as well as tending to isotropy (equal energy in all directions). The drift force quickly decreases with distance from the ice edge and, therefore, constitutes a local forcing effective near the ice edge only. Associated with this rapid decrease of the drift force, a large compressive stress develops that may be very important in compacting the floes in the vicinity of the ice edge.

To better understand this phenomenon, the wave-induced drift force has been computed as a function of distance from the ice edge, x, by including an exponential energy decay into (8);

$$F(x) = \int_0^{2\pi} \int_0^{\infty} E(f, \theta; x = 0) \times \exp(-\beta x/\cos\theta)\, \mathrm{Tr}(f) df \cos\theta d\theta \quad (13)$$

where $E(f, \theta; x = 0)$ is the incident spectrum, and β is the attenuation coefficient as given in Table 1. In Fig. 4, the total variance of the surface displacement

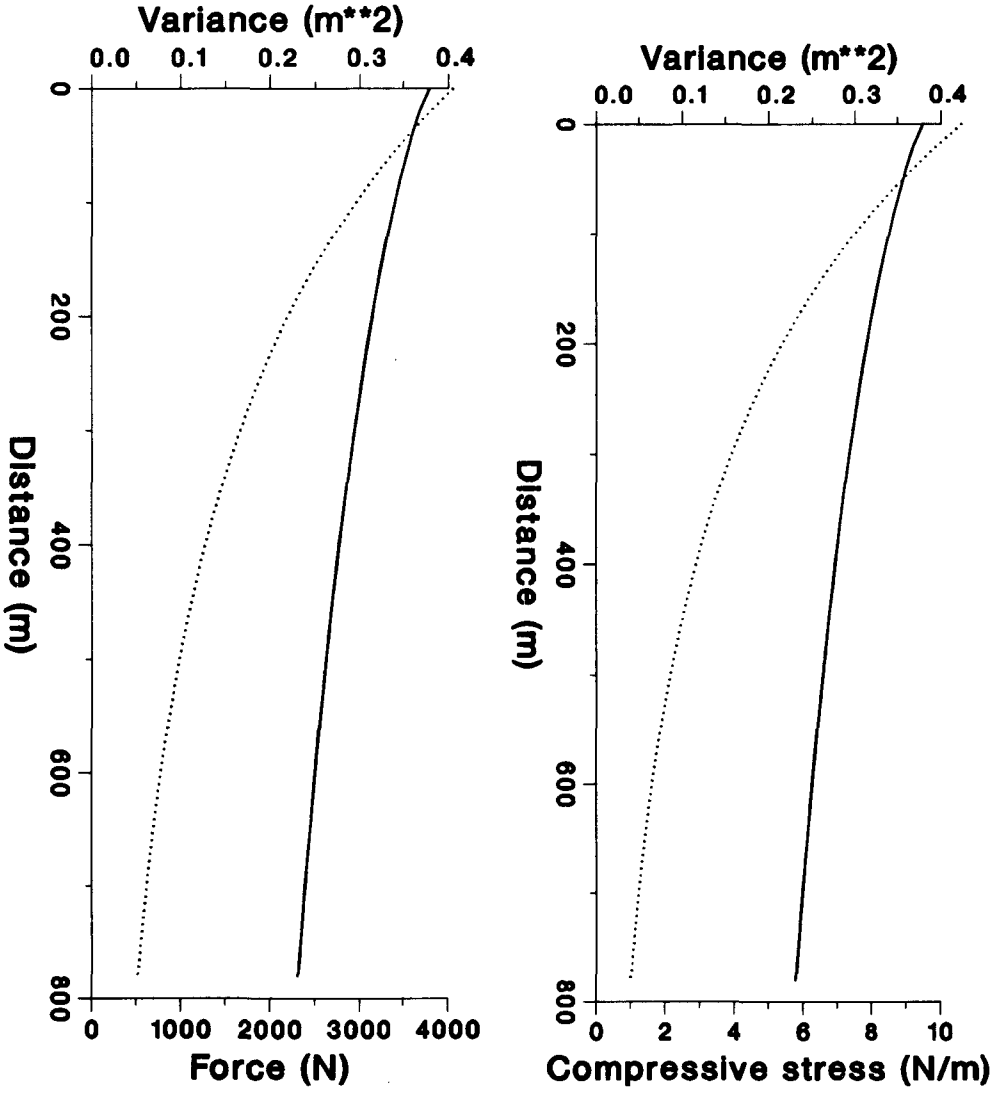

FIG. 4. Total variance (full line) with wave-induced drift force, (a), and compressive stress, (b), (dotted lines) against distance from the ice edge. The floes have a diameter of 10 m and a draft of 2 m.

is plotted against distance x, along with the total wave-induced drift force (Fig. 4a) and the compressive stress $dF(x)/dx$ (Fig. 4b). The computations have been performed for a floe of 10 m diameter and 2 m draft with an incident fully developed sea state ($U = 10$ m s^{-1}). The high values of the force (4.1×10^3 N) and of the compressive stress (10 N m^{-1}) at $x = 0$ rapidly decrease to half of their initial values at a distance just over 200 m from the ice edge. The directional broadening has not been included here because of a lack of an adequate parameterization, but its addition would result in an even faster decay of the drift force, and, consequently, in a higher compressive force concentrated closer still to the ice edge. This strong local compacting effect of the waves certainly plays an important role in the formation of a well-defined and highly compacted extreme ice edge commonly observed under on-ice wind conditions (e.g., Wadhams 1986).

4. Conclusion

The second-order wave-induced drift force on an axisymmetric floe in monochromatic waves has been presented in terms of a nondimensional transfer function. This function slowly increases as the horizontal dimension of the floe relative to the incident wavelength increases up to a point where the transfer function rapidly reaches its short-wave limit. The rapid change in the transfer function is associated with the occurrence of a resonant peak in the pitch response of the floe. The short-wave limit of the transfer function is determined by the shape of the horizontal floe contour and takes a maximum value of 2.0 and a reduced value of 1.33 for a square and a cylindrical flow, respectively. Using the computed values of the transfer function, the drift force was then computed for a series of directional wave spectra. Two situations in which the wave-induced drift may be important in the MIZ were analyzed: short waves generated in open water leads inside the ice cover, and open-water waves incident on the ice edge. The drift force due to the short waves present in polynyas, although reduced to just about half of what the 2D analysis predicts, may partly contribute to the formation of ice edge bands as proposed by Wadhams (1983). In the second situation, the high-frequency components of an open-water wave spectrum were shown to generate a large drift force on a floe directly exposed to them. However, because of the rapid decay of the short waves as they propagate into the ice cover, the large wave-induced drift force rapidly decays (in the first few hundred meters) and thus creates a strong local compressive force that compacts the ice at the extreme ice edge.

The simple analysis presented here of wave–ice interactions in the marginal ice zone, although not including all the processes involved, certainly provides insight into the complex problem. When floes are close to each other, the various floe–floe interactions, which have not been taken into account here, become important. Also, allowing for advecting floes would probably modify the results. Alternative approaches have been adopted by other authors to study the wave–ice interactions by either using the theory of flexural gravity waves (Wadhams 1973) or by modeling the ice cover as a highly viscous fluid (Weber 1987). The latter approach also suggests that the wave-induced stress may be very important in packing the ice.

The present results show that wave-induced drift force can play an important role in the local dynamics of the marginal ice zone near the ice edge and in situations where large open water leads are present.

REFERENCES

Bruno, M. S., and O. S. Madsen, 1989: Coupled circulation and ice floe movement model for partially ice-covered continental shelves. *J. Geophys. Res.*, **94,** 2065–2077.

Harms, V. W., 1987: Steady wave-drift of modeled ice floes. *Journal of the Waterway, Port, Coastal and Ocean Division,* **113,** 606–622.

Hasselmann, D. E., M. Dunckel and J. A. Ewing, 1980: Directional wave spectra observed during JONSWAP 1973. *J. Phys. Oceanogr.*, **10,** 1264–1280.

Hasselmann, K., T. P. Barnett, E. Bouws, H. Carlson, D. E. Cartwright, K. Enke, J. A. Ewing, H. Gienapp, D. E. Hasselmann, P. Kruseman, A. Meerburg, P. Muller, D. J. Olbers, K. Richter, W. Sell and H. Walden, 1973: Measurements of wind-wave growth and swell decay during the Joint North Sea Wave Project (JONSWAP). *Dtsch. Hydrogr. Z.*, **A8,** 95 pp.

Hsiung, C. C., and A. F. Aboul-Azm, 1982: Iceberg drift affected by wave action. *Ocean Eng.*, **9,** 433–439.

Isaacson, M. de St. Q., 1982: Fixed and floating axisymmetric structures in waves. *Journal of the Waterway, Port, Coastal and Ocean Division,* **108,** 180–199.

Jenkins, A. D., 1987: A dynamically consistent model for simulating near-surface ocean currents in the presence of waves. *Advances in Underwater Technology, Ocean Science, and Offshore Engineering,* Vol. 12. Graham and Trotman, 343–352.

Kobayashi, N., and S. Frankenstein, 1987: Wave drift force on ice floe. *Journal of the Waterway, Port, Coastal and Ocean Division,* **113,** 476–492.

Longuet-Higgins, M. S., 1977: The mean forces exerted by waves on floating or submerged bodies with applications to sandbars and wave power machines. *Proc. Roy. Soc. London,* **A352,** 463–480.

Maruo, H., 1960: The drift of a body floating on waves. *J. Ship Res.*, **4,** 1–10.

Masson, D., and P. H. LeBlond, 1989: Spectral evolution of wind-generated surface gravity waves in a dispersed ice field. *J. Fluid Mech.*, **202,** 43–81.

Newman, J. N., 1967: The drift and moment on ships in waves. *J. Ship Res.*, **11,** 51–60.

Smith, S. D., and N. R. Donaldson, 1987: Dynamic modeling of iceberg drift using current profiles. *Can. Tech. Rep. Hydrogr. Ocean Sci.*, **91,** 125 pp.

Wadhams, P., 1973: Attenuation of swell by sea ice. *J. Geophys. Res.*, **78,** 3552–3563.

——, 1983: A mechanism for the formation of ice edge bands. *J. Geophys. Res.*, **88,** 2813–2818.

——, 1986: The seasonal ice zone. *The Geophysics of Sea Ice,* N. Untersteiner, Ed., Plenum, 825–991.

——, V. A. Squire, J. A. Ewing and R. W. Pascal, 1986: The effect of the marginal ice zone on the directional wave spectrum of the ocean. *J. Phys. Oceanogr.*, **16,** 358–376.

Weber, J. E., 1987: Wave attenuation and wave drift in the marginal ice zone. *J. Phys. Oceanogr.*, **17,** 2351–2361.